Available online at www.sciencedirect.com
ScienceDirect
Journal of Non-Crystalline Solids 352 (2006) 5318–5324
JOURNAL OF NON-CRYSTALLINE SOLIDS
www.elsevier.com/locate/jnoncrysol

A case for local icosahedral order in undercooled metallic liquids and the influence on the nucleation barrier ☆

K.F. Kelton *, A.K. Gangopadhyay, T.H. Kim, G.W. Lee

Department of Physics, Washington University, Campus Box 1105, One Brookings Drive, St. Louis, MO 63130, USA

Received 16 August 2006
Available online 28 September 2006

Abstract

An overview of recent experimental and theoretical investigations on undercooled liquids is given, indicating developing short-range order with undercooling. Our in situ synchrotron X-ray diffraction studies of electrostatically levitated droplets of elemental Ti, Zr, and Ni liquids and coordinated undercooling and structural studies of a Ti–Zr–Ni liquid that forms an icosahedral quasicrystal are discussed in the context of these investigations. Icosahedral order is demonstrated to be a dominant component to the structures of all undercooled liquids studied, although it becomes significantly distorted with an increasing importance of the d-band bonding character. The liquid short-range order couples with the nucleation barrier, as predicted by Frank over a half-century ago.

PACS: 61.10.Nz; 61.20.−p; 64.60.Qb; 82.60.Nh

Keywords: Quasicrystals; Medium-range order

1. Introduction

Since 1724, when Fahrenheit performed the first recorded undercooling experiment on liquid water [1], it has been clear that an energy barrier separates the initial and final phases in a first order phase transformation. The stochastic thermally-activated transition over that barrier, i.e. nucleation, is typically analyzed within the classical theory of nucleation, a phenomenological model that describes the time-evolution of a size distribution of clusters of the new phase [2]. 'Homogeneous nucleation' is the most fundamental of the two types of nucleation, occurring randomly in space and time. 'Heterogeneous nucleation', is more common, occurring at specific sites in the initial phase.

Until the 1950s, it was not possible to significantly undercool liquid metals, suggesting that the barrier for the nucleation of the crystal phase was small. This appeared reasonable at the time, reflecting an assumed similar short range order in the two phases, supported by their similar densities and coordination numbers. As shown by Turnbull, however, the apparently small barrier was the result of heterogeneous nucleation, catalyzed by sample impurities and the surface container [3]. By rendering these heterogeneous nucleation sites ineffective, liquid metals could be supercooled by 20–30% of their melting temperatures before crystallizing. To explain this Frank pointed out that there exist three possible arrangements of twelve spheres in contact with a central sphere, the two close-packed crystal configurations (fcc and hcp) and an icosahedral packing, consisting of 20 slightly distorted tetrahedra around a common center [4]. For particles interacting under a central potential, such as the Lennard-Jones pair potential, the fully relaxed energy of the icosahedral cluster is lower than the crystal configurations. The point group symmetry of the icosahedral cluster, $m\bar{3}5$, is incompatible

☆ Paper presented at the 12th Liquids and Amorphous Metals Conference (LAM12), 11–16 July, 2004, Metz, France.

* Corresponding author. Tel.: +1 314 935 6228; fax: +1 314 935 6219.
E-mail address: kfk@wuphys.wustl.edu (K.F. Kelton).

0022-3093/$ - see front matter © 2006 Elsevier B.V. All rights reserved.
doi:10.1016/j.jnoncrysol.2006.08.009

with translational periodicity, however. If a large population of atoms in the undercooled liquid were in an icosahedral configuration, a natural barrier to the formation of small regions of the crystal phase would result – the nucleation barrier.

Molecular dynamics calculations generally support Frank's structural arguments. Steinhardt et al., for example, identified significant icosahedral order in an undercooled liquid of particles interacting via the Lennard-Jones potential [5,6]. This was determined from a set of rotationally invariant bond-orientational order parameters defined by expanding the density of bonds, ρ, on a unit sphere surrounding one of the atoms at position, r, in terms of spherical harmonics. The value of Q_6, corresponding to local icosahedral order, increases dramatically with undercooling, while the other Q_ℓ's change only slightly. Icosahedral order has also been inferred for Lennard-Jones glasses [7].

Recently direct experimental evidence for icosahedral order has been obtained from X-ray and neutron studies on levitated elemental and alloy metallic liquids, using electromagnetic [8,9] and electrostatic [10,11] levitation techniques. In one case [10] the evolving icosahedral order was directly linked to the nucleation of a metastable icosahedral quasicrystal, instead of the stable polytetrahedral C14 Laves phase, confirming Frank's hypothesis in that case. These studies are discussed in this manuscript and the experimental observations are demonstrated to be in agreement with recent modeling calculations made for more realistic atomic potentials. The consequences for nucleation theory, of the observed coupling of order parameter fluctuations in the metastable liquid with those corresponding to crystal nucleation, are discussed.

2. Experimental procedure

Small spheres (2–3 mm in diameter) of Ti–Zr–Ni alloys and of elemental Ti, Ni, and Zr were prepared by arc-melting on a water-cooled copper hearth in an argon (99.995%) atmosphere. High purity elemental materials were used, Ti (99.995%), Ni (99.995%), and Zr (99.95%, 3% Hf); the maximum concentrations of non-metallic impurities were C < 95 ppm, N < 20 ppm and O < 166 ppm.

To minimize the effects of heterogeneous nucleation, measurements of the liquid undercooling before crystallization were made using the electrostatic levitation facility (ESL) located at NASA/Marshall Space Flight Center [12]. The samples were positively charged with ultraviolet light and levitated in vacuum ($\approx 10^{-7}$ Torr) between electrostatic plates under a DC electric field (1–10 kV) as described elsewhere [13]. The samples were melted using a 50 W Nd-YAG laser or a 50 W CO_2 laser. Unlike electromagnetic levitation methods (EML), sample heating and positioning are decoupled in ESL, allowing a wider range of materials to be studied over a wider temperature range. Optical pyrometers with a 0.676 μm (Si) or 1.2–1.4 μm (In–Ga–As) wavelength range were used to measure the sample temperature to a relative accuracy of ±1 K. Emissivity values for the alloys were determined by matching the measured liquidus temperatures to known values and to values determined by differential thermal analysis.

By combining the containerless processing technique of electrostatic levitation (ESL) with X-ray synchrotron methods, it was possible to directly measure the structures of the undercooled liquids and to relate those to the nucleation barrier determined from the undercooling studies. The Beamline ESL (BESL) facility was developed through a joint collaboration between researchers from Washington University, NASA-Marshall Space Flight Center, and μ-CAT (beamline 6ID-D) at the Advanced Photon Source (APS) located at Argonne National Laboratory. A schematic diagram of BESL is shown in Fig. 1. Two separate Be windows were installed in the ESL chamber at diametrically opposite ends of the chamber for the entrance of the incident X-ray and exit of the diffracted beam. The diffracted beam was detected over a large q-range in less than one second using a MAR3450 image plate, allowing studies of the metastable liquid in the deeply undercooled state as well as the structural identification of transient solid phases that form during nucleation. High energy X-rays (125 keV, 0.099 Å) were used to provide a sufficiently wide scattering range and to minimize sample absorption and multiple scattering.

The diffracted intensities, $I(q)$, were extracted from the image plate data using *fit2D* (http://www.esrf.fr/computing/scientific/FIT2D/), a program designed for use with the MAR345 image plate. These data were corrected for scattering from the Be-windows and air outside the BESL chamber, obtained from scattering measurements made with no sample present. The $S(q)$ data were derived from the normalized intensity per atom in electron units, obtained from the measured scattering data after correcting for polarization, absorption, multiple scattering and Compton scattering, following standard procedures [14–16]. Due to the high count rates, the statistical quality of the scattering data is high. The background determination is the dominant contribution to an uncertainty in $S(q)$,

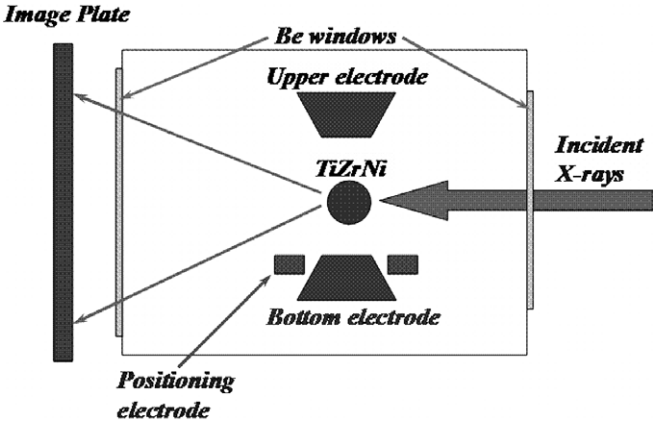

Fig. 1. Schematic diagram of the BESL facility (from [31]).

although the error is estimated to be of order the size of the data points in the figures shown.

3. Results

The $S(q)$ data for Ni, above and below the melting temperature, are shown in Fig. 2(a). For comparison, recently reported EML-based neutron diffraction results are also shown [9]; the agreement between the two sets of data is excellent. The dashed line shows the results of first principles calculations of $S(q)$ from the embedded atom method for the equilibrium liquid [17]. They give a reasonable prediction of the peak locations in $S(q)$, but predict different intensities. Of particular note is the failure to predict the shoulder on the high-q side of the second peak observed in the experimental data (indicated by the arrow), which becomes more prominent in the undercooled liquid.

The measured $S(q)$ for liquids of Ti are shown in Fig. 2(b). Earlier data obtained by Waseda are also shown (dotted line) [16,18] as well as the prediction of theoretical calculations (dashed line) [17]. These new data are significantly different from those from the earlier studies, but are in much better agreement with the theoretical results. Again, however, the second peak in $S(q)$ is wider than the theoretical prediction, owing to a shoulder on the high-q side. The shoulder is different than for Ni, however, comparable or greater in intensity than the second peak (inset of Fig. 2(b)). Further, unlike the data for Ni, the relative shapes and intensities of the second peak and shoulder in liquid Ti change little with increasing undercooling. As shown in Fig. 3, the $S(q)$ data for Zr as a function of temperature are more similar to the Ti data than to the Ni data (the Zr data are also in good agreement with recently reported neutron diffraction results [9]).

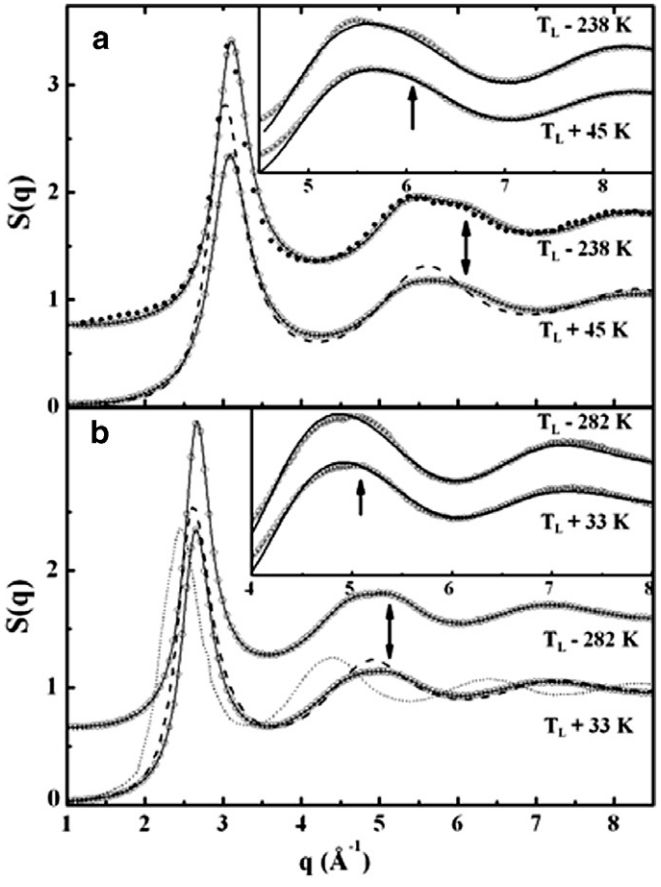

Fig. 2. X-ray structure factor for liquid Ni (liquidus temperature, $T_L = 1728$ K) (a) and Ti ($T_L = 1940$ K) (b) as a function of temperature; the curves are displaced vertically for clarity. (a) Dashed line from theory [17], closed circles from EML experiments [9] (selected data points are shown for clarity). (b) Dashed line from theory [17], dotted line from previous work [16,18]. Insets show fit to a 13-atom icosahedron (solid lines), above and below the melting temperatures (from [11]).

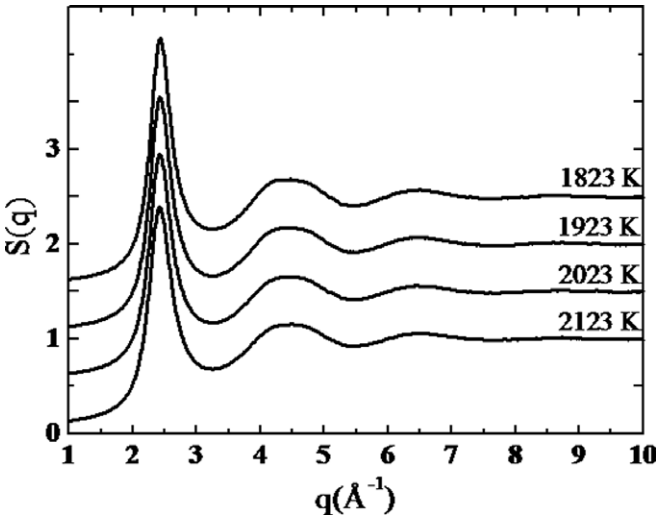

Fig. 3. X-ray structure factor for liquid Zr ($T_l = 2125$ K) as a function of undercooling.

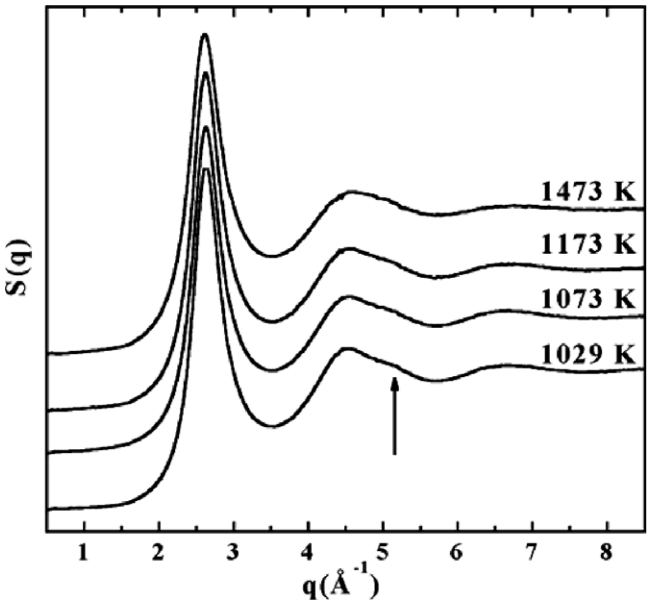

Fig. 4. $S(q)$ from the $Ti_{39.5}Zr_{39.5}Ni_{21}$ liquid as a function of temperature. The shoulder on the high-q side of the second peak (indicated by the arrow) becomes more prominent as the temperature is lowered below the liquidus temperature (1083 K) (taken from [10]).

Fig. 4 shows the X-ray structure factor as a function of undercooling temperature for a $Ti_{39.5}Zr_{39.5}Ni_{21}$ liquid that forms an equilibrium icosahedral quasicrystal phase, i-phase, at approximately 200 °C below the liquidus temperature [19]. The i-phase quasicrystal is a translationally ordered (but not periodic) phase with a non-crystallographic icosahedral symmetry. The equilibrium high-temperature phase in these alloys is the hexagonal C14 Laves phase, a polytetrahedral Frank–Kasper phase. As for the case of Ni, a shoulder on the high-q side of the second peak is evident even in the equilibrium liquid, becoming more prominent with increasing undercooling.

These $S(q)$ data demonstrate the significant development of short-range order with undercooling in metallic elemental and alloy liquids. In the elemental liquids the undercooling limit is set by the nucleation and growth of the equilibrium high temperature bcc phase in Ti and Zr and the fcc phase in Ni. A richer phase evolution occurs in the undercooled TiZrNi liquids.

For liquid metals, the growth velocities of the crystal phases are sufficiently large in the region of significant nucleation that the time scale for crystallization is dominated by the time required to form nuclei, producing a recalescence temperature where the released heat of transition causes a rapid rise in temperature. Fig. 5(a) shows the cooling curve for a levitated $Ti_{37}Zr_{42}Ni_{21}$ liquid, using ESL; the arrows mark the recalescence events. X-ray studies show that the first recalescence is due to the nucleation and growth of an i-phase (Fig. 5(b)), which is not stable in this temperature range. It transforms after 2–3 s (indicated by the second arrow) to another phase, which is identified as the C14 Laves phase (Fig. 5(b)).

The relative magnitudes of the nucleation barriers for different ordered phases scale with their reduced undercooling temperatures, $\Delta T_r = (T_l - T_r)/T_l = \Delta T/T_l$; T_l is the liquidus temperature (melting temperature for a pure element) and T_r is the recalescence temperature. Alloys that form the bcc solid solution phase, β(Ti/Zr) show the greatest amount of undercooling (Fig. 6), with the polytetrahedral C14 phase showing a lesser undercooling before recalescence and the i-phase showing the least.

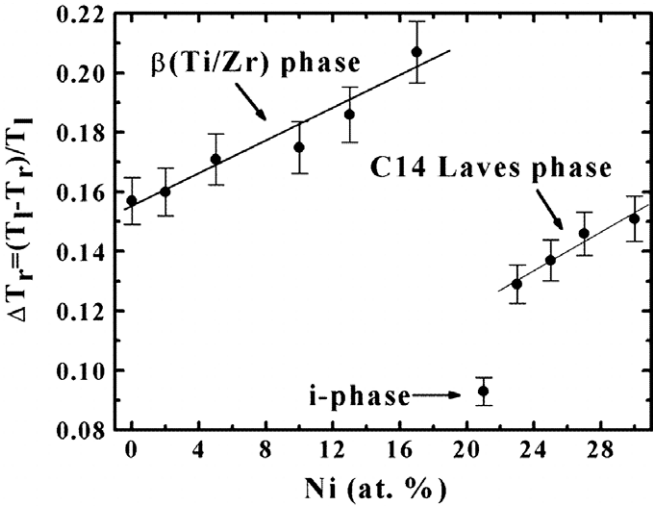

Fig. 6. Relative undercooling of $(TiZr)_{1-x}Ni_x$ liquids as a function of concentration and the primary crystallizing phases.

4. Discussion

While inert gas liquids are described reasonably well by hard sphere models, these models disagree with measured $S(q)$ data for transition metal liquids. Liquid structures obtained with more realistic pair potentials [17,20], agree reasonably well with the experimental results for the late transition metals (LTM), but fail for the early (Sc, Ti, V) transition metals (ETM), not even reproducing the correct $S(q)$ peak positions. These approaches do not properly account for the angular dependence of the transition metal potential and the tendency for the development of strong short range order in the liquid, particularly in alloys containing elements that have negative heats of mixing (such as Ni with Ti and Zr).

To lowest order, the liquid short-range order can be modeled by assuming tightly bound, non-interacting, close-packed, clusters. For the liquids discussed here, integrating over the first peak in the radial distribution function, obtained by a Fourier transformation of the measured $S(q)$, gave a coordination number of approximately 12,

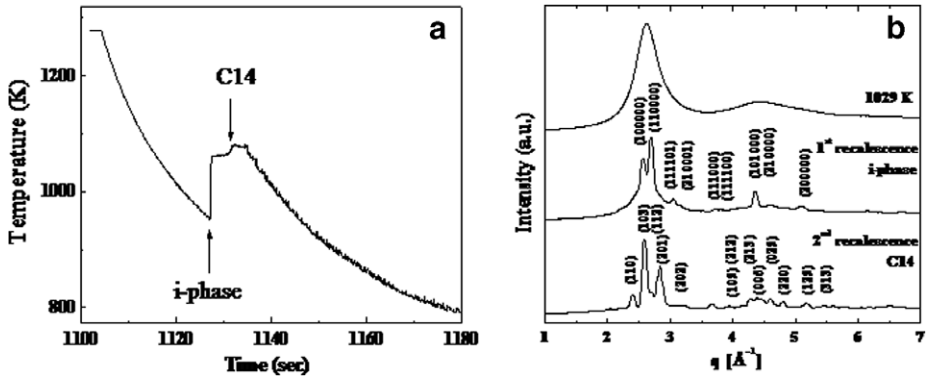

Fig. 5. (a) Cooling curves for electrostatically levitated 2.5 mm droplet of $Ti_{39.5}Zr_{39.5}Ni_{21}$ as a function of temperature showing two recalescence events (indicated by arrows). (b) X-ray diffraction pattern as a function of momentum transfer, q ($= 4\pi \sin\theta/\lambda$), for the undercooled liquid of Ti–Zr–Ni alloy at 1029 K, during the 1st recalescence to the i-phase, and during the 2nd recalescence to the C14 phase (taken from [10]).

consistent with a locally close-packed cluster structure (i.e., hcp, fcc or icosahedral clusters). Of these three, only the icosahedral cluster predicts the shoulder on the high-q side of the second peak in $S(q)$. Also, for Ni the ratios of the peak positions in $S(q)$, determined by fitting two overlapping Gaussian peaks, are $q(2nd)/q(1st) = 1.74 \pm 0.01$ and $q(shoulder)/q(1st) = 1.95 \pm 0.01$, in reasonable agreement with those expected for a perfect icosahedron (1.71 and 2.04, respectively) [21,22]. The $S(q)$ computed for a 13 atom icosahedral cluster agrees well with the experimentally measured peak locations and intensities when the Debye–Waller (DW) factors for atomic vibration within the cluster [9,10,23] are taken into account (inset of Fig. 2). The calculated DW factor, however, overestimates the temperature dependence, particularly at low temperature, causing the diminishment of the shoulder that is strongly present in the $S(q)$ for a static icosahedral cluster.

The growing prominence of the shoulder on the high-q side of the second peak of $S(q)$ indicates that the icosahedral short range order (ISRO) increases with undercooling, consistent with the results from molecular dynamics (MD) studies of atoms interacting by a Lennard-Jones (LJ) potential [5,6]. In those simulation studies, however, the ISRO vanishes above the melting temperature, whereas it persists up to the highest measurement temperature ($\sim$100 K above T_L) in the experimental data for liquid Ni. This possibly arises from some admixture of covalent character in the Ni bonds.

For Ti and Zr, the shoulder in $S(q)$ has approximately the same, or slightly larger, intensity as the second peak and changes little with temperature. This may be explained by distortions in the ISRO [11], perhaps signaling a growing importance of polytetrahedral order. It likely arises because of a competition between the icosahedral ordering, which maximizes density, and the greater influence of the angular dependence of the atomic potentials for Ti and Zr compared to Ni.

The ISRO in the $Ti_{39.5}Zr_{39.5}Ni_{21}$ alloys is likely favored by the strong heat of mixing for Ni with Ti and Zr, supported by a recently developed structural model for the TiZrNi i-phase [24]. Results from EML neutron diffraction studies of $Al_{13}(FeCo)_4$ alloys that form crystal approximant phases that are structurally closely related to the i-phase have also shown strong chemical ordering accompanying the development of icosahedral topological order [25].

The nucleation data for the Ti–Zr–Ni alloys in Figs. 5 and 6 provide strong additional support for the development of ISRO with undercooling in the TiZrNi alloys. The i-phase is clearly metastable, transforming to the stable C14 phase approximately 1–2 s after it has formed (Fig. 5). Within the classical theory of nucleation, the nucleation barrier (or work of critical cluster formation) is given by

$$W_{n^*} = A\frac{\sigma^3}{\delta\mu_v^2}, \tag{1}$$

where σ is the interfacial free energy between the liquid and the cluster of the ordered phase, $\delta\mu_v$ is the driving free energy for crystallization and A is a constant that depends on the geometry of the cluster ($A = 16\pi/3$ for spherical clusters). That the i-phase nucleates before the C14 phase, for which $\delta\mu_v$ is larger, demonstrates that the nucleation barrier is less for the i-phase, requiring that σ be smaller and correspondingly that the local structure of the liquid be closer to that of the i-phase than the C14 polytetrahedral phase. Taken together, then, the undercooling and the $S(q)$ data demonstrate that for a Ni concentration of 21 at.%, the local structure of the liquid is dominated by local icosahedral order, and not some other form of polytetrahedral order. For low Ni alloys, the $S(q)$ data are similar to those for Ti (Fig. 2) and Zr (Fig. 3), consistent with distorted local icosahedral configurations, possibly having a more polytetrahedral character. Regardless of the perfection of the icosahedral order in the liquid with low Ni concentration, however, the nucleation barrier for the β(Ti/Zr) remains high and the observed increasing ΔT_r with increasing Ni concentration reflects the decreasing liquidus temperature [26]. Since the liquidus temperatures for alloys with [Ni] concentrations greater than 21 at.% vary little, however, the increasing ΔT_r for the C14 phase with increasing Ni signals an increasing nucleation barrier. This suggests that with increasing Ni concentration above 21 at.%, the local liquid configuration becomes less icosahedral, although not developing a local polytetrahedral order that would be favorable for the easy nucleation of the C14 phase.

A 13 atom icosahedron is the simplest cluster that can be used to reproduce the essential features in $S(q)$ that are associated with icosahedral order. However, it is unlikely to be the proper structural unit for the liquid. Studies of Ti–Zr–Ni quasicrystals have shown that they are based on packings of Bergman-type clusters, containing 33 and 45 atoms [24,27]. In fact, Schenk et al. argued that their $S(q)$ data for liquid Ni were best fit by a 33 atom dodecahedron [9]. Given the uncertainty in the DW factor, however, it is difficult to decide which icosahedral-type cluster is best. Likely, the liquid phase contains cluster fragments, some with icosahedral symmetry, some with distorted icosahedral symmetry, some with a polytetrahedral symmetry, and some with other symmetries, probably even crystallographic ones. These structures are likely stochastic in time, forming and breaking apart on a time scale shorter than the X-ray diffraction studies. The collective data from ESL and EML experimental studies, however, demonstrate that the dominant time-averaged local structure is icosahedral in many Al- and Ti/Zr-based liquids.

This conclusion is consistent with recent molecular dynamics studies using realistic atomic potentials. Considering an ensemble of 400,000 Al atoms interacting under a generalized non-local pseudopotential, Dong et al. found that more than 88% of the atoms in the liquid belong to well defined clusters of different types [28]. Four indices characterized each cluster type [29]; the first index denotes to which peak of $g(r)$ the pair (called the root pair) belongs to, the second gives the number of near neighbors shared by the root pair, the third gives the number of nearest-neighbor bonds

among the shared neighbors and the fourth index is to distinguish configurations that have the same first three indices but different topology. In their calculations, most atoms were associated with clusters with tetrahedral and icosahedral symmetry; the densities of these are shown in Fig. 7 as a function of undercooling temperature. Diagrams of the icosahedral and select tetrahedral clusters are also shown in the figure; the white circles represent atoms in the root pair and the black circles represent near-neighbor atoms that belong to both of the white circle atoms. Cluster 1551 corresponds to perfect icosahedral order, 1541 to distorted icosahedral order and clusters 1421, 1422, 1431 and 1441 to tetrahedral order. From Fig. 7 the bond types in clusters 1541 and 1551 are dominant over all temperatures, indicating that the liquid has local ISRO even at the melting temperature, although there the ISRO is distorted. With decreasing temperature, however, undistorted ISRO becomes increasingly dominant, while the density of all other configurations remain approximately constant, in agreement with our $S(q)$ data for the Ni and TiZrNi liquids. In agreement with our Ti and Zr data, showing features that are characteristic of distorted icosahedral order, ab initio MD calculations for Zr liquids indicate that the ISRO decreases slightly (both 1551 and 1541) while the tetrahedral order increases [30]. Surprisingly, these calculations also indicate that a significant number of atoms are arranged in symmetries characteristic of crystalline order.

The combined structural and undercooling data for TiZrNi demonstrate that the influence of preexisting local order in the liquid is important in dictating the pathway for the liquid/solid phase transition. Taking measured values for the heat of fusion and viscosity ($\Delta H_f = 8.1$ kJ/mol, $\eta = 0.00718\exp[696.91/(T - 791.12)]$ poise, unpublished) and an interfacial free energy estimated from the maximum undercooling, the diameter of the critical size calculated from the classical theory of nucleation is approximately 3.8 nm at the recalescence temperature (953 K). The coherence length estimated from the width of the first peak is approximately 2.1 nm at 1029 K, the lowest temperature for which $S(q)$ could be measured. It appears, then, that the icosahedral order in the liquid is acting as a template, catalyzing the nucleation of the icosahedral phase. The growing ISRO will increase the barrier to nucleation of the crystal phase, in opposition to the decrease expected with the larger driving free energy associated with deeper undercooling (Eq. (1)).

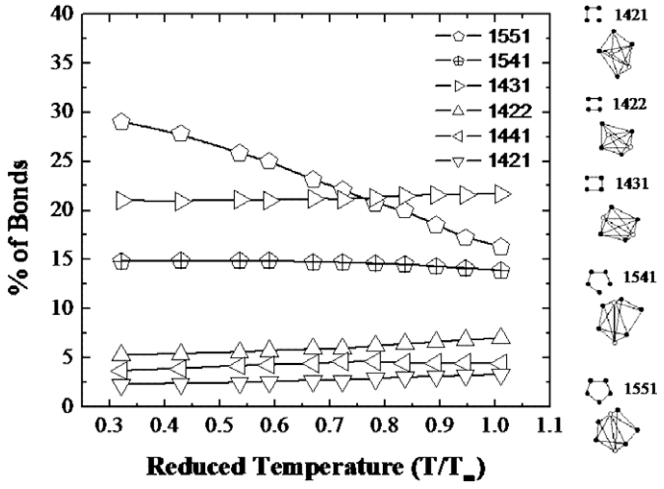

Fig. 7. Fraction of bond types from MD calculation for Al, computed from data in [28]. Cluster types for ISRO (1551 and 1541) and tetrahedral order are shown (see text for description of indexing scheme).

5. Conclusions

Scattering studies of containerlessly processed elemental transition metal and alloy liquids demonstrate an increasing short-range order with undercooling. In many cases, this corresponds to an increase in the number of atoms in an icosahedral configuration. With increasing importance of the angular dependence of the atomic potential, however, the ISRO becomes distorted, likely becoming more tetrahedral in character and possibly developing a crystallographic-type local order. These experimental results are supported by molecular dynamics simulations for large ensembles of atoms interacting under realistic potentials.

In TiZrNi alloys, the growing ISRO decreases the nucleation barrier for the icosahedral quasicrystal. This example of a coupling between the structural fluctuations in the initial phase and the fluctuations leading to the nucleation of the final phase blurs the distinction between homogeneous and heterogeneous nucleation when the initial and final phases have similar local to intermediate structural order. While not surprising that the local structures of strongly bonded liquids or polymers influence the phases that form, the same is true in metallic liquids, although the atomic interactions are weaker and more isotropic. Although confirming Frank's hypothesis, the local order in the liquid need not necessarily be identified with interfacial energy. A full treatment of coupled-order parameter nucleation processes will require a shift of emphasis from parameters such as the interfacial free energy, which is difficult to define accurately for small clusters, to an order parameter approach, such as incorporated in density functional treatments.

Acknowledgments

The liquid diffraction data cited were taken in collaboration with J. Rogers, T.J. Rathz, R.W. Hyers, A.I. Goldman and D.S. Robinson and were reported previously in references [10] and [11]. The authors thank A.L. Greer and D. Holland-Moritz for useful discussion. The work at Washington University was supported by the National Aeronautics and Space Administration under Contract NCC 8-85 and the National Science Foundation under Grants DMR 00-72787 and DMR 03-07410. The use of the Advanced Photon Source was supported by the US DOE, Basic Energy Sciences, Office of Science, under

Contract No. W-31-109-Eng-38 and MUCAT by Contract No. W-7405-Eng-82 through the Ames Laboratory.

References

[1] D.B. Fahrenheit, Philos. Trans. Roy. Soc. 33 (1724) 78.
[2] K.F. Kelton, in: H. Ehrenreich, D. Turnbull (Eds.), Solid State Physics, 45, Academic Press, Boston, 1991, p. 75.
[3] D. Turnbull, J. Chem. Phys. 20 (1952) 411.
[4] F.C. Frank, Proc. Roy. Soc. London A 215 (1952) 43.
[5] P.J. Steinhardt, D.R. Nelson, M. Ronchetti, Phys. Rev. Lett. 47 (1981) 1297.
[6] P.J. Steinhardt, D.R. Nelson, M. Ronchetti, Phys. Rev. B 28 (1983).
[7] F. Yonezawa, in: H. Ehrenreich, D. Turnbull (Eds.), Solid State Physics, vol. 45, Academic, Boston, 1991, p. 179.
[8] D. Holland-Moritz, T. Schenk, V. Simonet, R. Bellissent, P. Convert, T. Hansen, J. Alloys Compd. 342 (2002) 77.
[9] T. Schenk, D. Holland-Moritz, V. Simonet, R. Bellissent, D.M. Herlach, Phys. Rev. Lett. 89 (2002) 075507.
[10] K.F. Kelton, G.W. Lee, A.K. Gangopadhyay, R.W. Hyers, T. Rathz, J. Rogers, M.B. Robinson, D. Robinson, Phys. Rev. Lett. 90 (2003) 195504.
[11] G.W. Lee, A.K. Gangopadhyay, K.F. Kelton, R.W. Hyers, T.J. Rathz, J.R. Rogers, D. Robinson, Phys. Rev. Lett. 93 (2004) 037802.
[12] J.R. Rogers, R.W. Hyers, T. Rathz, L. Savage, M.B. Robinson, in: Paper Presented at the Proceedings of the Space Technology and Applications International Forum, Albuquerque, NM, 2001.
[13] A.J. Rulison, J.L. Watkins, B. Zambrano, Rev. Sci. Instrum. 68 (1997) 2853.
[14] C.N.J. Wagner, Liquid Metals; Chemistry and Physics, Marcel Dekker, New York, 1972.
[15] B.E. Warren, X-ray Diffraction, Dover, New York, 1990.
[16] Y. Waseda, The Structure of Non-Crystalline Materials, McGraw-Hill, New York, 1980.
[17] G.M. Bhuiyan, M. Silbert, M.J. Stott, Phys. Rev. B 53 (1996) 636.
[18] Y. Waseda, S. Tamaki, Philos. Mag. 32 (1975) 273.
[19] G.-W. Lee, T.K. Croat, A.K. Gangopadhyay, K.F. Kelton, Philos. Mag. Lett. 82 (2002) 199.
[20] C. Hausleitner, G. Kahl, J. Hafner, J. Phys. 3 (1991) 1589.
[21] S. Sachdev, D.R. Nelson, Phys. Rev. Lett. 53 (1984) 1947.
[22] S. Sachdev, D.R. Nelson, Phys. Rev. B 32 (1985).
[23] V. Simonet, F. Hippert, H. Klein, Phys. Rev. B 58 (1998) 6273.
[24] R.G. Hennig, M. Mihalkovic, K.F. Kelton, C.L. Henley, Phys. Rev. B 67 (2003) 134202.
[25] T. Schenk, V. Simonet, D. Holland-Moritz, R. Bellissent, T. Hansen, P. Convert, D.M. Herlach, Europhys. Lett. 65 (2004) 34.
[26] K.F. Kelton, Mater. Sci. Eng. A 375–377 (2004) 31.
[27] R.G. Hennig, E.H. Majzoub, A.E. Carlsson, K.F. Kelton, C.L. Henley, W.B. Yelon, S. Misture, Mater. Sci. Eng. A 294–296 (2000) 361.
[28] K.J. Dong, R.S. Liu, A.B. Yu, R.P. Zou, J.Y. Li, J. Phys. D: Conden. Matter 15 (2003) 743.
[29] J.D. Honeycutt, H.C. Andersen, J. Chem. Phys. 91 (1987) 4950.
[30] N. Jakse, A. Pasturel, Phys. Rev. Lett. 91 (2003) 195501.
[31] C. Day, Phys. Today 56 (2003) 24.